JMEMS Letters

Periodic Array of Subwavelength MEMS Cantilevers for Dynamic Manipulation of Terahertz Waves

Prakash Pitchappa, Chong Pei Ho, Lokesh Dhakar, You Qian, Navab Singh, *Senior Member, IEEE*, and Chengkuo Lee, *Member, IEEE*

***Abstract*— We experimentally demonstrate the active manipulation of terahertz (THz) waves using a periodic array of electrostatically actuated subwavelength microelectromechanical system cantilevers, which effectively behave like a metamaterial. The design methodology for achieving desired ON- and OFF-state resonance frequencies through electromechanical optimization is presented. The microcantilever metamaterial has a switching range of 0.29 THz and a modulation depth of 60% at 0.59 THz. Utilizing metal layer thickness to optimize the devices, an improvement of 40% is achieved in switching range. The microcantilever metamaterials are highly miniaturized, extremely scalable, and electrically controlled with attractive electro-optic performance. Multiple cantilevers can be placed in a desired fashion to form complex unit cell geometry to realize advanced THz manipulation, such as polarization switching, bandwidth tunable filters, multicolor imagers, and so on. [2015-0090]**

***Index Terms*— Digital metamaterial, MEMS metamaterial, microcantilevers, reconfigurable, switchable, terahertz.**

I. Introduction

Terahertz (THz) region of the electromagnetic (EM) spectrum has a great potential in the realization of wide range of impactful applications, such as non-invasive medical inspection, next-generation wireless communication networks, non-destructive fault analysis, security surveillance, etc. [1]–[4]. Micromachining has enabled THz based optical devices such as waveguides and antennas [5]. However, the interaction of THz waves with naturally occurring materials is very minimal and this has greatly hindered the realization of high-performance THz devices and its potential application scope. Recently, EM metamaterials (MM) with the possibility to achieve desired EM properties by engineering subwavelength pattern geometry has immensely helped to bridge the so-called “THz gap” (0.1-10 THz). These EM properties of MMs are determined primarily by the pattern size and shape. Therefore, active restructuring of these pattern geometry provides the most straightforward and efficient way for dynamic control of MM response [6]–[8].

Manuscript received March 31, 2015; accepted April 7, 2015. Date of publication April 30, 2015; date of current version June 1, 2015. This work was supported by the Ministry of Education, Singapore, through the Academic Research Fund Tier 2 under Grant MOE2012-T2-2-154 within the National University of Singapore, Singapore. Subject Editor O. Solgaard.

P. Pitchappa and C. P. Ho are with the Department of Electrical and Computer Engineering, National University of Singapore, Singapore 117576, and also with the Institute of Microelectronics, Agency for Science, Technology, and Research, Singapore 117685.

L. Dhakar, Y. Qian, and C. Lee are with the Department of Electrical and Computer Engineering, National University of Singapore, Singapore 117576 (e-mail: elelc@nus.edu.sg).

N. Singh is with the Institute of Microelectronics, Agency for Science, Technology, and Research, Singapore 117685.

Color versions of one or more of the figures in this letter are available online at http://ieeexplore.ieee.org.

Digital Object Identifier 10.1109/JMEMS.2015.2421307

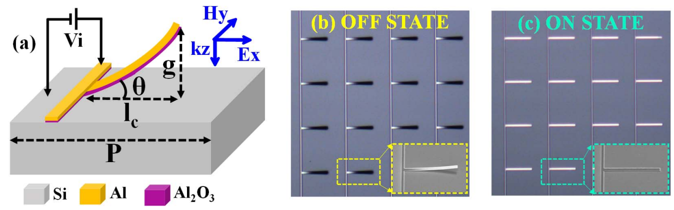

Fig. 1. (a) Schematic drawing of an upward bent microcantilever as metamaterial unit cell with geometrical parameter definition. OM images of the fabricated microcantilever metamaterial array in (b) OFF state and (c) ON state, respectively. Inset shows the SEM image of the metamaterial unit cell in their corresponding state.

Microelectromechnical system (MEMS) based actuators realized using well established micromachining technologies enables the active restructuring of MM unit cell geometries. Various types of MEMS actuators have been reported for active THz MM, such as comb drives [9], thermal bimorphs [10], out-of-plane deformable cantilevers [11]–[14] and electrostatically actuated fixed-fixed beams [15]. Pre-stressed cantilevers integrated into complex metamaterial unit cell geometry has been recently reported for various optical functionalities, such as dynamic magnetic and electrical switching, multiband switching etc. [11]–[13]. In the presented approach, the simplest unit cell in cantilever-based approach is a single microcantilever. The detailed study and design principle of these MMs will provide a comprehensive understanding of cantilever-based MMs (CMM). This will form the building blocks which will enable the design of more complex unit cells, desired for advanced THz functionalities such as anisotropy switching, bandwidth tunable MMs, active chiral MMs, etc.

II. Device Design

The proposed CMM consists of array of cantilevers with period ‘P’, cantilever length ‘l_c’ and width ‘w_c’, as shown in Fig. 1(a). Each cantilever is a bimorph structure formed by aluminum (Al) of ‘t_{Al}’ thickness on top of aluminum oxide (Al_2O_3) dielectric layer of thickness ‘t_d’. The microcantilever array was fabricated on 8-inch silicon wafer using CMOS compatible process with silicon-di-oxide as the sacrificial layer [10]. After the vapor hydrofluoric acid (VHF) release step, the bimorph cantilevers bends up due to the residual stress in Al/Al_2O_3 layers with maximum air gap ‘g’ between the tip of released cantilevers and Si substrate as shown in Fig 1(b). The radius of curvature of the released cantilever ‘r’ [16] is given by:

$$\frac{1}{r} = \frac{6n(1+n)(m\sigma_{Al} - \sigma_d)}{t_{Al} E_{Al}[K + 3mn(1+n^2)]}$$

where $K = 1 + 4mn + 6mn^2 + 4mn^3 + m^2n^4$;

$$m = E_{Al}/E_d; \quad n = t_{Al}/t_d;$$

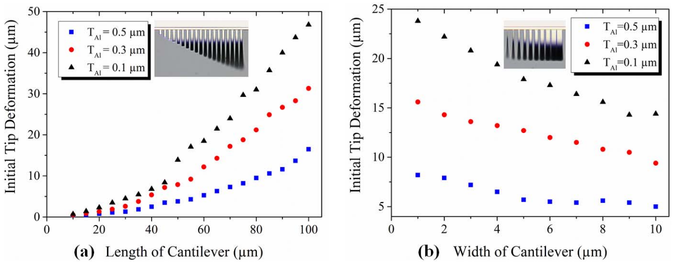

Fig. 2. Measured initial tip displacement for bimorph cantilevers for three different thickness of Al -0.5 μm (blue-square), 0.3 μm (red-circle), 0.1 μm (black-triangle) and fixed Al_2O_3 thickness of 50 nm with (a) varying cantilever length at fixed width of 5 μm and (b) varying cantilever width at fixed length of 60 μm, respectively.

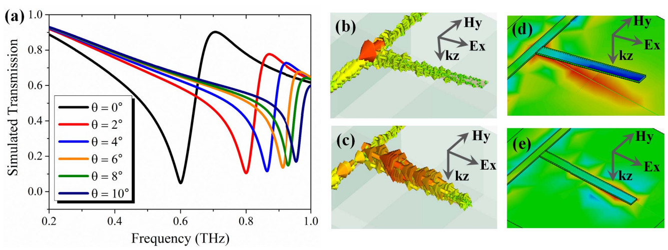

Fig. 3. (a) Simulated transmission spectra for CMM with varying release angle (θ) for the THz incident with electric field along the length of the cantilever (X direction). Simulated surface current configuration for (b) $\theta = 10°$ at 0.97 THz (OFF State) and (c) $\theta = 0°$ at 0.6 THz (ON State). Z-component of scattered electric field at (d) 0.97 THz for $\theta = 10°$ (OFF State) and (e) $\theta = 0°$ at 0.6 THz (ON State), respectively.

The tip displacement can be calculated as: $\delta = r[1 - \cos(\frac{l_c}{r})]$ where, E_{Al} and E_d is the Young's modulus and σ_{Al} and σ_d is the residual stress of Al and Al_2O_3 material layers, respectively. The measured tip displacement of bimorph cantilevers increases rapidly with increase in length and decrease in t_{Al} thickness as shown in Fig. 2(a). However, with increasing width, the tip displacement decreases linearly up to where the w_c/t_{Al} ratio is 10. Further increase in width has minimal influence in the tip displacement as shown in Fig. 2(b).

The resonant frequency of the metamaterial can be modeled as an equivalent circuit model, whose resonant frequency is given by $\omega_r = (L_{eff}C_{eff})^{-1/2}$. The equivalent inductance, $L_{eff} \propto \mu_0 t_{Al} w_c/l_c$ and equivalent capacitance, C_{eff} is given by two capacitances, the capacitance due to dielectric Al_2O_3, $C_d \propto \varepsilon_0\varepsilon_r w_c l_c/t_d$, and the capacitance due to air gap, $C_g \propto \varepsilon_0 w_c l_c/g$. In order to elucidate the resonance mechanism and study the effect of various geomertical parameters variation on ω_r, finite-difference time-domain (FDTD) simulations were carried out. Fig. 3(a) shows that the CMM ω_r is strongly blue-shifted with increasing air-gap 'g'. The induced surface current in the microcantilever at $\theta = 10°$ and 0° is along the same direction as the incident electric field as shown in Fig. 3(b) and 3(c), respectively. This clearly suggests the excitation of first-order dipolar mode resonance of cut wire MMs. The Z-component of the scattered electric field shows a strong coupling of incident electric field to the CMM for both $\theta = 10°$ and 0° as shown in Fig. 3(d) and Fig. 3(e), respectively. Hence as g decreases, C_g and hence C_{eff} will decrease, thereby shifting ω_r to higher frequencies.

For active reconfiguration, the out-of-plane air gap, 'g' is changed using electrostatic force by applying voltage across the released cantilevers and Si substrate. When the applied voltage is higher than the critical pull-in voltage, the cantilevers will come into physical contact with Si substrate, i.e. $g = 0$ ($\theta = 0°$) [17]. The Al_2O_3 dielectric layer

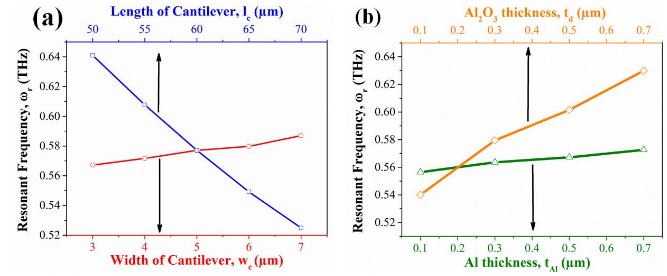

Fig. 4. (a) Simulated resonance frequency of microcantilever metamaterial at $\theta = 0°$ (ON State) with (a) varying cantilever length (red) and cantilever width (blue) and (b) varying Al thickness (green) and varying Al_2O_3 thickness (orange), respectively.

beneath the Al layer in the cantilevers will prevent the current flow between the cantilevers and Si substrate after snap down. Based on the position of the cantilevers, two states for CMM are defined. The state when the cantilevers are released and no voltage is applied is termed as "OFF" state and the state in which the cantilevers are in physical contact with the Si substrate after applying pull-in voltage (V_{PI}) is termed as "ON" state as shown in Fig. 1(b) and 1(c), respectively.

In case of cantilever length variation, as l_c increases both L_{eff} and C_{eff} increases, and so causes ω_r to red-shift as shown in Fig 4(a). On the other hand, with increasing cantilever width, both C_{eff} and L_{eff} are reduced thereby causing the ω_r to slightly blue-shift as shown in Fig 4(a). For the t_{Al} variation, ω_r slightly blue-shifts with increasing t_{Al} as shown in Fig 4(b). Finally, when t_d is increased, C_d will decrease and hence C_{eff} will also decrease, thereby causing a blue-shift in ω_r accordingly. As a design principle, first the cantilever length ($l_c = 60$ μm) and width ($w_c = 5$ μm) are designed based on the desired $\omega_{r\text{-}ON}$ (0.6 THz). And as $\omega_{r\text{-}OFF}$ is strongly dependent on intial tip displacement, either the Al or Al_2O_3 thickness can be varied. As Al_2O_3 is deposited using atomic layer deposition process, Al thickness is varied to achieve desired initial tip displacment and hence corresponding $\omega_{r\text{-}OFF}$ values. However, this also means that achieving higher values of $\omega_{r\text{-}OFF}$, through reduction of Al thickness will be limited by the skin depth of Al in THz region ($t_{Al} < 100$ nm).

III. Characterization

Three CMMs with varying Al thickness of 100 nm, 300 nm and 500 nm were fabricated and are termed as A100, A300 and A500 as shown in Fig. 5(a-c), respectively. The initial tip displacement was measured to be approximately 20.2 μm, 10.2 μm and 5.5 μm, with corresponding pull-in voltage of 35V, 40V and 45V, respectively. The THz transmission spectra is measured using THz-time domain spectroscopy (TDS) system. The incoming wave is incident normally with electric field along the length of cantilevers onto the sample placed in the nitrogen-filled chamber. Fig. 6(a) shows the measured transmission spectra for A100, A300 and A500 devices in ON and OFF states (normalized with respect to bare Si substrate). The $\omega_{r\text{-}OFF}$ and $\omega_{r\text{-}ON}$ for A500 is at 0.88 THz and 0.59 THz, respectively and fits quite well with the simulation results shown in Fig 3(a). Owing to the increased initial tip displacement of A300 and A100 devices, the OFF state resonant frequency is observed at 0.935 THz and 0.96 THz. The $\omega_{r\text{-}ON}$ for A300 and A100 is slightly red-shifted to 0.587 THz and 0.56 THz, respectively when compared to $\omega_{r\text{-}ON}$ of A500 (0.59 THz). This can be attributed to the reduced thickness of Al layer.

The increase in $\omega_{r\text{-}OFF}$ can be considered as an improvement in switching range and is calculated to be ~40% higher for A100, compared to A500 device. The improvement in switching range

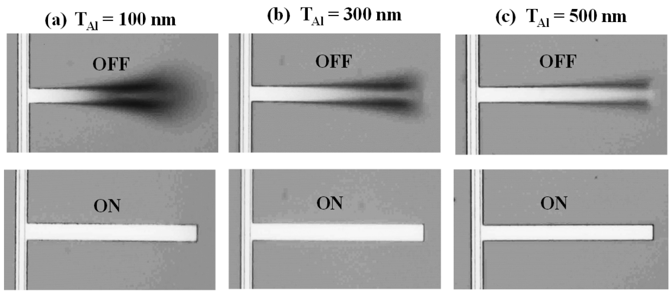

Fig. 5. OM images of CMM unit cell in OFF and ON state with Al thickness, t_m = (a) 100 nm, (b) 300 nm and (c) 500 nm, respectively. The out-of-focus along the cantilever in OFF state clearly shows the increased tip displacement for lower Al thickness. In ON state the entire cantilever is in focus, hence confirms the physical contact with Si substrate for all CMMs. The direction of the incident THz electric and magnetic field for all measurement is shown in (a) and the direction of propagation is normal to the cantilever structures.

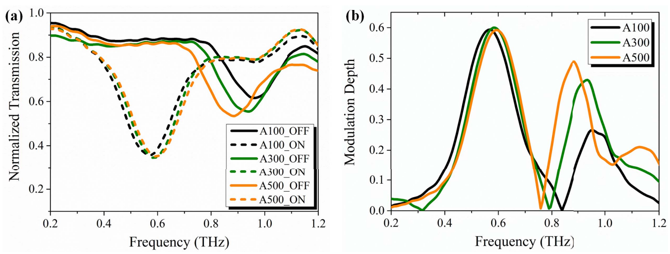

Fig. 6. (a) Measured THz transmission spectra for THz waves incident with E field along the cantilever length for fabricated devices A100 (black), A300 (green) and A500 (yellow) devices in OFF (solid lines) and ON states (dashed lines). (b) Calculated modulation depth for A100 (black), A300 (green) and A500 (yellow), respectively.

of ~0.11 THz is much higher than the tuning range of most non-MEMS based tunable methods. The modulation depth is calculated as $MD = |T_{ON}\text{-}T_{OFF}|/T_{OFF}$ and is shown in Fig. 6b. All three metamaterials shows dual band modulation characteristics with maximum modulation depth of 0.6 at their respective $\omega_{r\text{-}ON}$. At $\omega_{r\text{-}OFF}$, the modulation depth for A500, A300 and A100 is around 0.5, 0.4 and 0.25, respectively. These devices with the modulation depth of 60% is highly attractive for applications such as sub-THz wireless signal switching [4], single-pixel THz imaging where currently 30% contrast is utilized [18] and as digital bit for programmable metamaterial [19].

IV. Conclusion

In summary, we demonstrate the array of sub-wavelength microcantilever for efficient switching of terahertz waves, towards the realization of electrically controlled digital metamaterials. It has a maximum switching range of 0.29 THz and modulation depth of 60% at 0.59 THz. By reducing the metal thickness from 500 nm to 100 nm, the switching range was improved by 40%. Cantilever-based metamaterial approach provides the ideal platform for realizing numerous advanced THz functionalities by placing multiple cantilevers in the desired way to form more complex metamaterial unit cell. These metamaterials with high electro-optic performance such as switching range and modulation depth, simple design, extreme scalability and realized using CMOS compatible process are highly attractive for terahertz based next-generation high-speed communication and non-invasive medical devices.

References

[1] M. Shur, "Terahertz technology: Devices and applications," in *Proc. 31st Eur. Solid-State Circuits Conf. (ESSCIRC)*, Sep. 2005, pp. 13–21.
[2] P. H. Siegel, "Terahertz technology in biology and medicine," in *IEEE MTT-S Int. Microw. Symp. Dig.*, vol. 3. Jun. 2004, pp. 1575–1578.
[3] E. Pickwell and V. P. Wallace, "Biomedical applications of terahertz technology," *J. Phys. D, Appl. Phys.*, vol. 39, no. 17, pp. R301–R310, Aug. 2006.
[4] S. Koenig *et al.*, "Wireless sub-THz communication system with high data rate," *Nature Photon.*, vol. 7, no. 12, pp. 977–981, Oct. 2013.
[5] V. M. Lubecke, M. Mizuno, and G. M. Rebeiz, "Micromachining for terahertz applications," *IEEE Trans. Microw. Theory Techn.*, vol. 46, no. 11, pp. 1821–1831, Nov. 1998.
[6] J. M. Zendejas, J. P. Gianvittorio, Y. Rahmat-Samii, and J. W. Judy, "Magnetic MEMS reconfigurable frequency-selective surfaces," *J. Microelectromech. Syst.*, vol. 15, no. 3 pp. 613–623, Jun. 2006.
[7] A. Q. Liu, W. M. Zhu, D. P. Tsai, and N. I. Zheludev, "Micromachined tunable metamaterials: A review," *J. Opt.*, vol. 14, no. 11, p. 114009, Sep. 2012.
[8] H. Tanoto, L. Ding, and J. H. Teng, "Tunable terahertz metamaterials," *Int. J. THz. Sci. Technol.*, vol. 6, no. 1, pp. 1–25, Mar. 2013.
[9] W. M. Zhu *et al.*, "Microelectromechanical Maltese-cross metamaterial with tunable terahertz anisotropy," *Nature Commun.*, vol. 3, Dec. 2012, Art. ID 1274.
[10] H. Tao, A. C. Strikwerda, K. Fan, W. J. Padilla, X. Zhang, and R. D. Averitt, "Reconfigurable terahertz metamaterials," *Phys. Rev. Lett.*, vol. 103, no. 14, p. 147401, Oct. 2009.
[11] Y.-S. Lin, Y. Qian, F. Ma, Z. Liu, P. Kropelnicki, and C. Lee, "Development of stress-induced curved actuators for a tunable THz filter based on double split-ring resonators," *Appl. Phys. Lett.*, vol. 102, no. 11, pp. 111908-1–111908-5, Mar. 2013.
[12] F. Ma, Y.-S. Lin, X. Zhang, and C. Lee, "Tunable multiband terahertz metamaterials using a reconfigurable electric split-ring resonator array," *Light, Sci. Appl.*, vol. 3, no. 5, pp. e171-1–e171-8, May 2014.
[13] C. P. Ho, P. Pitchappa, Y.-S. Lin, C.-Y. Huang, P. Kropelnicki, and C. Lee, "Electrothermally actuated microelectromechanical systems based omega-ring terahertz metamaterial with polarization dependent characteristics," *Appl. Phys. Lett.*, vol. 104, no. 16, p. 161104, Apr. 2014.
[14] Z. Han, K. Kohno, H. Fujita, K. Hirakawa, and H. Toshiyoshi, "MEMS reconfigurable metamaterial for terahertz switchable filter and modulator," *Opt. Exp.*, vol. 22, no. 18, pp. 21326–21339, Aug. 2014.
[15] M. Unlu, M. R. Hashemi, C. W. Berry, S. Li, S.-H. Yang, and M. Jarrahi, "Switchable scattering meta-surfaces for broadband terahertz modulation," *Sci. Rep.*, vol. 4, Jul. 2014, Art. ID 5704.
[16] R. T. Chen, H. Nguyen, and M. C. Wu, "A low voltage micromachined optical switch by stress-induced bending," in *Proc. 12th IEEE Int. Conf. Micro Electro Mech. Syst. (MEMS)*, Jan. 1999, pp. 424–428.
[17] R. Legtenberg, J. Gilbert, S. D. Senturia, and M. Elwenspoek, "Electrostatic curved electrode actuators," *J. Microelectromech. Syst.*, vol. 6, no. 3 pp. 257–265, Sep. 1997.
[18] C. M. Watts *et al.*, "Terahertz compressive imaging with metamaterial spatial light modulators," *Nature Photon.*, vol. 8, pp. 605–609, Jun. 2014.
[19] T. J. Cui, M. Q. Qi, X. Wan, J. Zhao, and Q. Cheng, "Coding metamaterials, digital metamaterials and programmable metamaterials," *Light, Sci. Appl.*, vol. 3, no. 10, pp. e218-1–e218-9, Oct. 2014.